Analytical Linescan Model for SEM Metrology

Chris A. Mack[a], Benjamin D. Bunday[b]
[a]Lithoguru.com, 1605 Watchhill Rd, Austin, TX 78703, E-mail: chris@lithoguru.com
[b]SEMATECH, Albany, NY, 12203, USA

Abstract

Critical dimension scanning electron microscope (CD-SEM) metrology has long used empirical approaches to determine edge locations. While such solutions are very flexible, physics-based models offer the potential for improved accuracy and precision for specific applications. Here, Monte Carlo simulation is used to generate theoretical linescans from single step and line/space targets in order to build a physics-based analytical model. The resulting analytical model fits the Monte Carlo simulation results for different feature heights, widths, and pitches. While more work is required to further develop this scheme, this model is a candidate for a new class of improved edge detection algorithms for CD-SEMs.

Subject Terms: Scanning electron microscope, SEM, linescan model, critical dimension, JMONSEL, CD-SEM, edge detection

1. Introduction

Scanning electron microscopes (SEMs) are commonly used to measure critical dimensions (CDs) during semiconductor manufacturing. A very narrow beam of electrons hits the sample at one location, interacting with the sample to scatter, lose energy, and generate secondary electrons that do the same. A positively biased detector(s) measures electrons that escape from the sample, either backscattered electrons (with higher energies), secondary electrons (with lower energies), or both, depending on the detector configuration. Scanning the position of the beam and recording the number of detected electrons at each position (pixel), a top-down image of the sample is constructed. Analysis of the image is often used to measure properties of the sample, such as the width of a feature (the CD). Extracting information about a sample from an image of the sample is a class of problems called the "inverse" problem, where the process of imaging is calculated in reverse. Inverse problems can be solved easily if the imaging process is not too complex or if high accuracy is not required, but can become exceeding difficult when high accuracy is desired for complex processes. Such is the case for analysis of SEM images.

The difficulty of the inverse problem can be understood by performing the forward calculations, that is, by simulating an image from a given, known sample. For SEM imaging, this involves the use of a Monte Carlo style of simulation, since the interaction of electrons with a sample has major random components. In this work, a Monte Carlo simulator for SEM image prediction called JMONSEL was used.[1-3] The very nature of such Monte Carlo calculations makes inverse calculations virtually impossible. Thus, most solutions to this inverse problem involve overly simplified approaches that take little or no account of the physics of SEM image formation: image smoothing coupled with edge detection techniques such as threshold edge detection.[4] These techniques, with much study and refinement, have proven adequate for the most part. However, as feature sizes shrink and the demands for accurate measurements scale with those sizes, current methods may no longer suffice.[5,6]

An approach that has seen some success is model-based library matching.[7-12] In this technique, the forward-calculated imaging model is used to generate a library of images over a range of expected samples (different feature types and sizes of the desired materials). When an experimental image is captured, it is matched to the closest library image (possibly using interpolation between images), which is then assumed to represent an accurate description of the experimental sample. While effective, the model-based library approach suffers from the computational burden of generating a sufficiently robust library of images and a lack of flexibility to make up for library incompleteness.

In this work, a third path is taken, somewhat intermediate between image processing that does not take the physics of image formation into account, and model-based library generation that is completely physics-based. Here a simplified analytical linescan model (ALM) will be derived, inspired by the physics of electron-sample interactions (though still quite empirical in nature).[13] The ALM will prove similar to the model proposed by Frase, who used the same basic approach adopted in this work.[14] The ALM will be calibrated by fitting to Monte Carlo simulations of SEM images. Once a set of ALM parameters has been calibrated, this new linescan model can be fit to experimental SEM images as a sort of physics-based edge detection algorithm. While much work remains to be done to prove out this approach, preliminary results are quite encouraging.

2. Simulation of Scanning Electron Micrograph Linescans

The first step in developing a simplified analytical linescan model is to generate a series of calculated SEM images from known sample structures. Simulations of SEM images were performed using JMONSEL (**J**ava **Mon**te Carlo Simulator of **S**econdary **El**ectrons), a program developed at the National Institute of Standards and Technology (NIST).[1-3] JMONSEL is used here as a "virtual SEM", where the user can input idealized structures from a limited list of materials, with perfect user-defined geometries. The user can also define SEM parameters such as the number of incident electrons per pixel, pixel size, spot size, and beam energy. While the program can also account for charging phenomena in and around the sample and fields created by the detector, these effects were neglected in the simulations performed for this study.

The virtual samples consisted of isolated edges (steps) and line/space patterns of various sizes and pitches on a uniform substrate. Features were made of either silicon or poly(methyl methacrylate) (PMMA), both on a planar silicon substrate. PMMA was chosen as a reasonable approximation of photoresist. Further, the sidewall angle of the edge or feature was varied between 45° and 91°. The landing energy was set at 500 eV and a point beam of electrons was used at each pixel location (with the effect of a larger beam size to be included later). Near the line edge, a pixel size of 0.1 nm was used. For most simulations N = 25,000 incident electrons per pixel were simulated. An example linescan is shown in Figure 1.

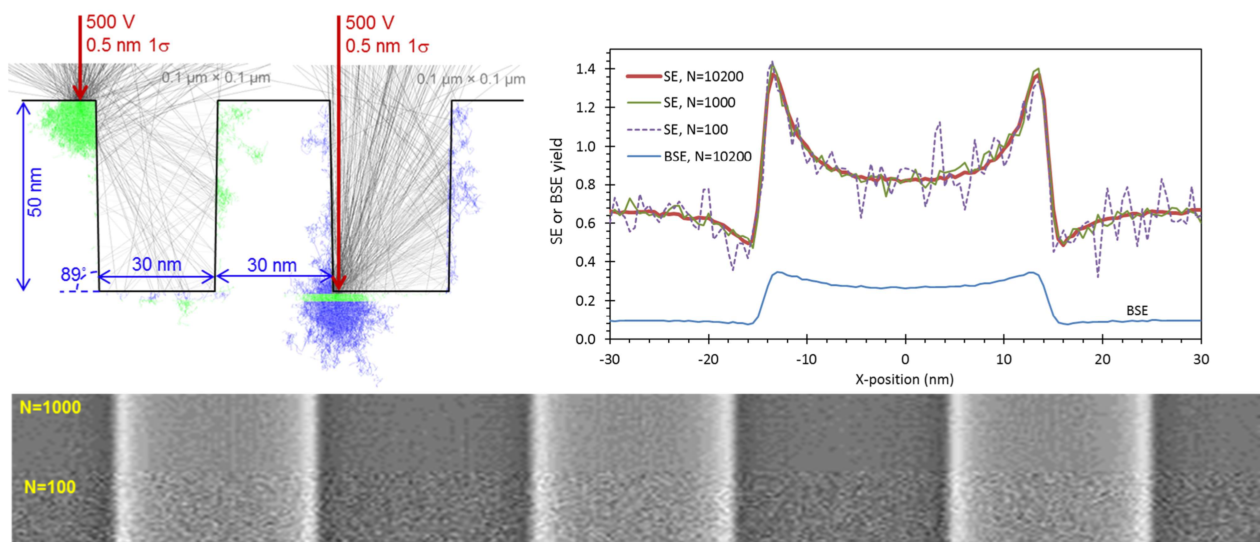

Figure 1. Example outputs from JMONSEL. Top-left: Simulated trajectories in a 30 nm line/space Si-on-thin SiO_2 structure at 500 V and 0.5 nm incident spot (one standard deviation Gaussian profile), where the interaction volumes can be seen at feature tops and bottoms. Top-right: Example linescan, including waveforms for secondary electron (SE) and backscatter electron (BSE) yields. SE electrons are defined as having energies ≤ 50 eV, with BSE electrons defined as having energies > 50 eV. Bottom: Simulated image of same waveform for N=1000 (top) and N=100 (bottom). Figure from Ref. 13.

3. Derivation of an Approximate Linescan Model for an Isolated Edge

Our previous work began the process of deriving a simple analytical linescan model.[13] Here that model will be explained, expanded, and refined. While the approach and model proposed by Frase[14] is very similar, there are some differences. The linescan, corresponding to the detected secondary electrons, will be $SE(x)$. Consider first a bare silicon wafer (corresponding to when the scan beam is a long way from any feature edge). Inside the silicon we can assume that the energy deposition profile takes the form of a double Gaussian, with a forward scattering width and a fraction of the energy forward scattered, and a backscatter width and a fraction of the energy deposited by those backscattered electrons. We will also assume that the number of secondary electrons that are generated within the wafer are in direct proportion to the energy deposited per unit volume, and the number of secondary electrons that escape the wafer (and so are detected by the SEM) are in direct proportion to the number of secondaries generated near the very top of the wafer.

The secondary electrons that reach the detector will emerge some distance r away from the position of the incident beam. From the assumptions above, the number of secondaries emerging from the substrate will be a function of r as

$$f(r) = ae^{-r^2/2\sigma_f^2} + be^{-r^2/2\sigma_b^2} \tag{1}$$

where σ_f and σ_b are the forward and backscatter ranges, respectively. The integration of this function over all space will be the linescan signal at $x = -\infty$ (a long way from an isolated edge located at x = 0). Carrying out this integration in polar coordinates,

$$SE(-\infty) = \int_0^{2\pi} d\theta \int_0^{\infty} f(r) r dr = 2\pi\left(a\sigma_f^2 + b\sigma_b^2\right) \tag{2}$$

Now consider the effect of an isolated step located at $x \geq 0$ (see Figure 2). Before looking at a silicon or PMMA step, imagine a completely absorbing step that does not allow the release of secondary electrons. In other words, all electrons that travel up into the step material simply disappear. For $x < 0$, we can calculate the reduction in the SE signal by calculating the number of absorbed secondaries as

$$SE_{absorbed}(x) = 2\int_0^{\pi/2} d\theta \int_{r_0}^{\infty} f(r) r dr \tag{3}$$

where $r_0 = x/\cos(\theta)$. Carrying out the integration,

$$SE_{absorbed}(x) = \pi a\sigma_f^2\left[2 - erfc\left(\frac{x}{\sigma_f\sqrt{2}}\right)\right] + \pi b\sigma_b^2\left[2 - erfc\left(\frac{x}{\sigma_b\sqrt{2}}\right)\right] \tag{4}$$

The linescan signal for $x < 0$ will be

$$\frac{SE(x)}{SE(-\infty)} = 1 - \frac{SE_{absorbed}(x)}{SE(-\infty)} = \left(\frac{1}{2} - \beta\right) erfc\left(\frac{x}{\sigma_f\sqrt{2}}\right) + \beta\, erfc\left(\frac{x}{\sigma_b\sqrt{2}}\right) \tag{5}$$

where $\beta = \frac{\pi b\sigma_b^2}{SE(-\infty)} = \frac{b\sigma_b^2}{2\left(a\sigma_f^2 + b\sigma_b^2\right)}$ and $\frac{1}{2} - \beta = \frac{a\sigma_f^2}{2\left(a\sigma_f^2 + b\sigma_b^2\right)}$.

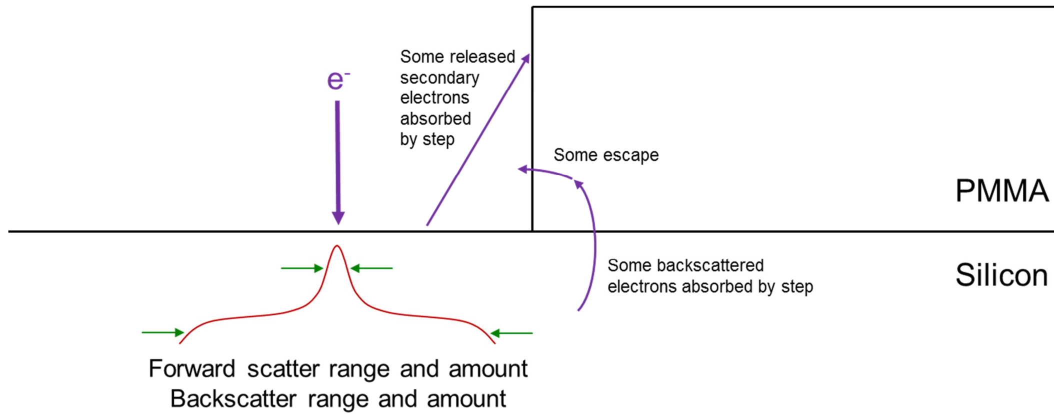

Figure 2. Geometry and physical interpretation of wafer part of the analytical linescan model (ALM) derived in this paper, showing a PMMA edge on a silicon wafer.

In what will follow, the complimentary error functions will prove cumbersome. However, since they are only used for $x < 0$ they can be approximated with exponentials with good-enough accuracy (the maximum error is less than 5%, occurring at a distance of $x/\sigma = -1.7$).

$$\text{For } x < 0, \quad erfc\left(\frac{x}{\sigma\sqrt{2}}\right) \approx 2 - e^{x/\sigma} \tag{6}$$

giving

$$\frac{SE(x)}{SE(-\infty)} = 1 - \left(\frac{1}{2} - \beta\right) e^{x/\sigma_f} - \beta e^{x/\sigma_b} \tag{7}$$

We can now see how this model matches the rigorous Monte Carlo simulations of the linescan for the case of a 50-nm tall silicon edge at 500 V landing energy, using a point incident beam. Figure 3 shows the best fit of equation (7) to the simulation results. The best fit parameters are $\sigma_f = 1.73$ nm, $\sigma_b = 40.4$ nm, and $\beta = 0.22$. The equation matches the simulations for the most part within the noise of the simulations (though some small systematic deviations can be observed), and the resulting parameters make intuitive sense for the scattering of 500 eV electrons in silicon.

The assumption of an absorbing step is not completely accurate for silicon, and even less so for a step made of photoresist. In reality, backscatter electrons travel up into the step and generate secondaries that can escape from the sidewall of the step. As a result, the step may not absorb all of the electrons entering, and in fact may generate more secondaries than if no step were present. Further, the step may absorb electrons that escape the surface of the wafer near the step before those electrons can travel to the detector (see Figure 2). These variations can be accommodated by simply modifying the forward scatter and backscatter step absorption terms in equation (7).

$$\text{For } x < 0, \quad \frac{SE(x)}{SE(-\infty)} = 1 - \alpha_f e^{x/\sigma_f} - \alpha_b e^{x/\sigma_b} \tag{8}$$

where α_f is the fraction of forward scatter-generated secondaries absorbed by the step and α_b is the fraction of backscatter-generated secondaries absorbed by the step. Note that if the presence of the step results in more secondary electrons escaping to the detector, then the result will be a negative value of α. In our previous work,[13] the $x < 0$ linescan model of equation (8) was compared to the Monte Carlo simulations for the cases of an isolated 50-nm tall

vertical (90º) silicon step on a silicon wafer and for a 50-nm tall vertical (90º) PMMA step on silicon, with landing voltages of 300, 500, and 800 V. The fits of the model to the simulations were within the random variations present in the Monte Carlo results (using 5000 incident electrons per pixel), with the best-fit parameters shown in Table I.

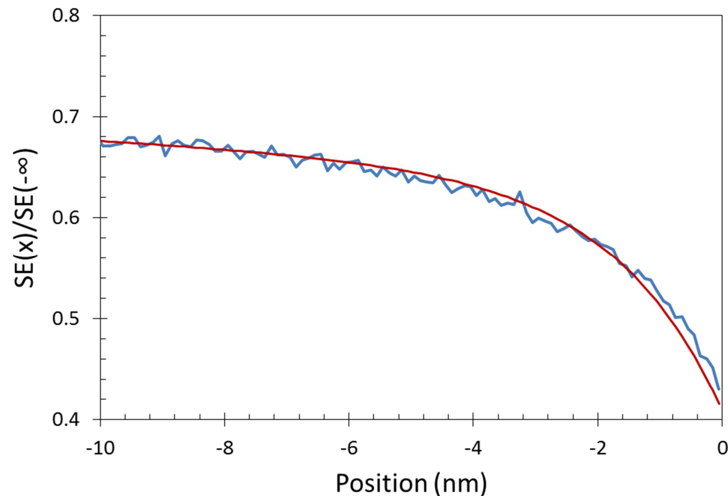

Figure 3. Best fit of equation (7) to rigorous Monte Carlo simulations of a 50-nm tall silicon edge at 500 eV landing energy, using a point incident beam, when $x < 0$ (that is, on the bottom half of the step). The smooth (red) line is the equation and the jagged (blue) line is the Monte Carlo simulation.

Table I. Best fit parameters of equation (8) to rigorous Monte Carlo simulations of an isolated 50-nm tall silicon step and PMMA step on a silicon wafer at 300, 500, and 800 V electron voltage, using a point incident beam, for $x < 0$ (from Ref. 13).

	Electron Landing Voltage		
	300V	500V	800V
Si wafer background signal, $SE(-\infty)$	1.070	0.818	0.597
Si forward scatter range, σ_f (nm)	1.37	2.31	3.96
Si backscatter range, σ_b (nm)	43.5	43.0	43.7
Si step forward scatter absorption, α_f	0.223	0.243	0.267
Si step backscatter absorption, α_b	0.251	0.212	0.171
PMMA step forward scatter absorption, α_f	0.272	0.316	0.363
PMMA step backscatter absorption, α_b	0.055	-0.047	-0.162

Expanding on these prior results, the step height was varied from 10 nm to 100 nm for the case of a 500 V incident beam, but now using 25,000 incident electrons per pixel for increased precision. The results are shown in Figures 4 – 6, for each of the parameters of the model. The error bars represent the range of the parameter that keeps the RMS fit error within 5% of its best fit value, holding all other parameters constant. (Thus, these error bars do not represent standard errors of the parameters since the do not account for correlations between parameters).

Examining these results one can draw two major conclusions. First, as Figure 6 shows, the backscatter range parameter σ_b varies linearly with step height. Taller steps influence the linescan out to a distance away from the edge

about equal to the step height, indicating that the major mechanism of SE absorption by the step comes from secondaries released from the wafer surface that strike the step sidewall. Second, all other parameters are essentially constant for step heights greater than about 20 nm for both silicon and PMMA steps. This 20-nm "threshold" thickness is expected to be a function of voltage, becoming thicker for voltages greater the 500 V, and thinner for voltages less than 500 V.

When $x > 0$, the incident beam is on top of the step. A model similar to that described for the bottom of the step can be applied to the top, but with some differences. The edge of the step does not absorb the long-range backscattered electrons, and in fact enhances the release of secondaries created by the forward scattered electrons. Thus, we will add a positive term $\alpha_e e^{-x/\sigma_e}$ to account for the enhanced escape of forward-scattered secondaries where σ_e is very similar to the forward scatter range of the step material. When the incident beam is very close to the step, however, the interaction volume of the forward-scattered electrons with the material is reduced, causing the generation of less secondaries. Thus, we subtract a term $\alpha_v e^{-x/\sigma_v}$ where $\sigma_v < \sigma_e$. This gives our linescan expression for the top of the step:

$$\text{For } x > 0, \quad \frac{SE(x)}{SE(\infty)} = 1 + \alpha_e e^{-x/\sigma_e} - \alpha_v e^{-x/\sigma_v} \tag{9}$$

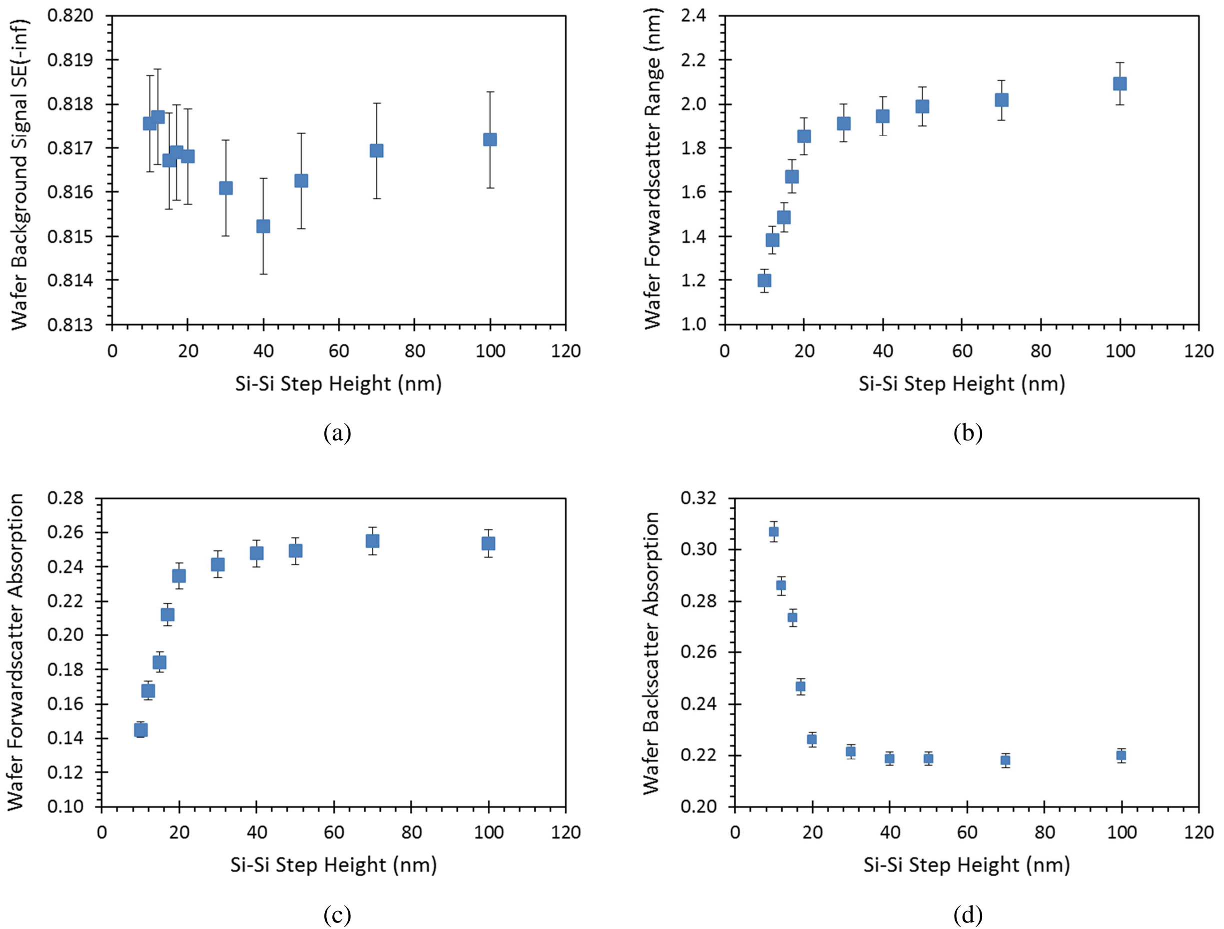

Figure 4. Best fit parameters of equation (8) to rigorous Monte Carlo simulations of an isolated silicon edge at 500 eV landing energy, using a point incident beam, when $x < 0$ (that is, on the bottom half of the step) for various step heights. All parameters are shown here except the wafer backscatter range σ_b, which is shown in Figure 6.

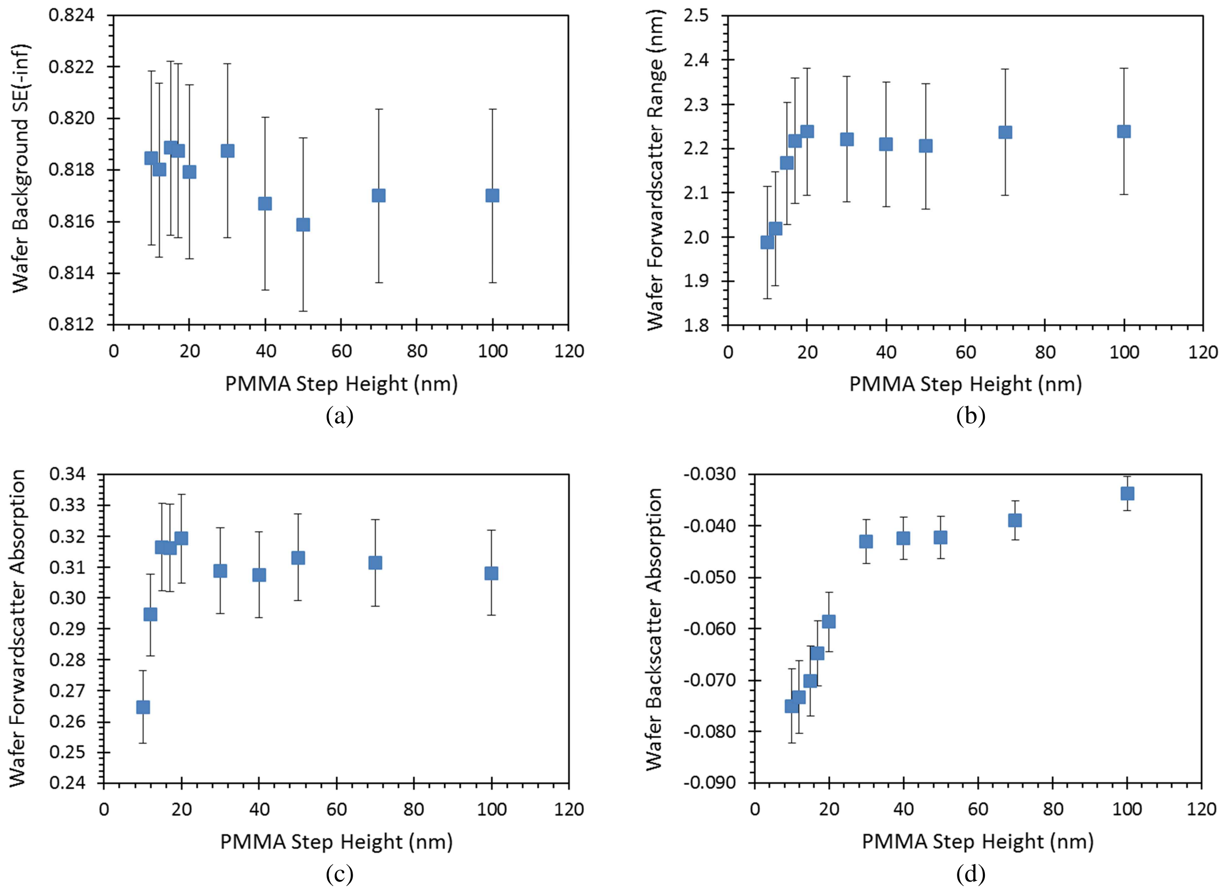

Figure 5. Best fit parameters of equation (8) to rigorous Monte Carlo simulations of an isolated PMMA edge at 500 eV landing energy, using a point incident beam, when $x < 0$ (that is, on the bottom half of the step) for various step heights. All parameters are shown here except the wafer backscatter range σ_b, which is shown in Figure 6.

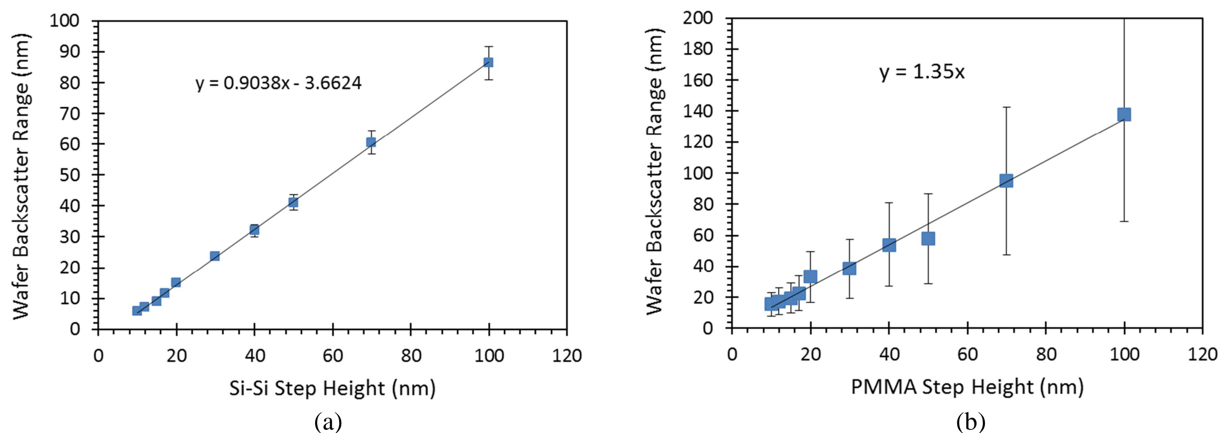

Figure 6. Best fit of the wafer backscatter range σ_b of equation (8) to rigorous Monte Carlo simulations of (a) a silicon edge, and (b) a PMMA edge on a silicon wafer at 500 eV landing energy, using a point incident beam, when $x < 0$ (that is, on the bottom half of the step) for various step heights.

In our previous work,[13] the $x > 0$ linescan model of equation (9) was compared to the Monte Carlo simulations for the cases of an isolated 50-nm tall vertical (90º) silicon step on silicon and for a 50-nm tall vertical (90º) PMMA step on silicon, with landing voltages of 300, 500, and 800 V. The fits of the model to the simulations were within the random variations present in the Monte Carlo results (using 5000 incident electrons per pixel), with the best-fit parameters shown in Table II.

Table II. Best fit parameters to rigorous Monte Carlo simulations of an isolated 50-nm tall silicon step and PMMA step on a silicon wafer at 300, 500, and 800 V electron landing voltage, using a point incident beam (from Ref. 13).

	Electron Landing Voltage		
	300V	500V	800V
Si step forward scatter range, σ_e (nm)	1.47	2.64	4.65
Si step volume loss range, σ_v (nm)	0.40	0.27	0.11
Si step edge enhancement factor, α_e	1.61	1.65	1.87
Si step volume loss factor, α_v	0.924	0.660	0.543
PMMA step forward scatter range, σ_e (nm)	3.42	3.54	5.28
PMMA step volume loss range, σ_v (nm)	0.53	1.43	2.39
PMMA step edge enhancement factor, α_e	0.382	1.427	2.784
PMMA step volume loss factor, α_v	0.347	1.143	1.968
PMMA background signal, $SE(\infty)$	2.286	2.132	1.552

Expanding on these results, the step height was varied from 10 nm to 100 nm for the case of a 500 V incident beam, using 25,000 incident electrons per pixel. The results are shown in Figures 7 – 8, for each of the top-of-the-step parameters of the model. Examining these results, all the parameters remain approximately constant for silicon or PMMA step heights greater than about 20 nm.

Combining the $x < 0$ and $x > 0$ linescan expressions into one expression (using the unit step function, $u(x)$), we have a final linescan expression for the case of a point incident beam and a vertical isolated step.

$$SE(x) = SE(-\infty)\left[1 - \alpha_f e^{x/\sigma_f} - \alpha_b e^{x/\sigma_b}\right]u(-x) + SE(\infty)\left[1 + \alpha_e e^{-x/\sigma_e} - \alpha_v e^{-x/\sigma_v}\right]u(x) \tag{10}$$

Next, the sidewall angle of the steps was varied from 45° to 91°. As an extreme case, 45° isolated 20-nm and 50-nm tall silicon steps produce the simulated linescans shown in Figure 9. The linescans can be broken up into three regions: to the left of the bottom of the edge (corresponding to the wafer, and represented by the linescan function of equation (8)), to the right of the top of the edge (represented by the linescan function of equation (9)), and the middle region corresponding to the sloped edge itself. Thus, a new linescan function for this middle region is required.

Examining Figure 9, the middle of the sidewall region has a steady secondary electron signal, which we will call SE_{edge}, at a higher level than the background wafer. This signal level then falls to the bottom level over a characteristic distance δ_1 at the bottom of the step, and rises to the top level over a characteristic distance δ_2 at the top of the step, forming an S-shaped waveform. Defining $x = 0$ to be the bottom (left) edge of a step of height h and sidewall angle θ, the top (right) edge will be at $x = h/\tan\theta$. A reasonable model for the linescan in this step region will be

$$SE(x) = SE_{edge} + \left(SE(-\infty)\left[1-\alpha_f - \alpha_b\right] - SE_{edge}\right)e^{-x/\delta_1} + \left(SE(+\infty)\left[1+\alpha_e - \alpha_v\right] - SE_{edge}\right)e^{-(h/\tan\theta - x)/\delta_2} \tag{11}$$

Here, $h/\tan\theta$ is assumed to be large compared to δ_1 and δ_2, but simple modifications to equation (11) can be made if this is not the case. Equation (11) applies to sidewall angles less than 90º. For small amounts of profile undercut ($\theta > 90$º), the resulting linescan can still be fit using the linescan function of equation (10).

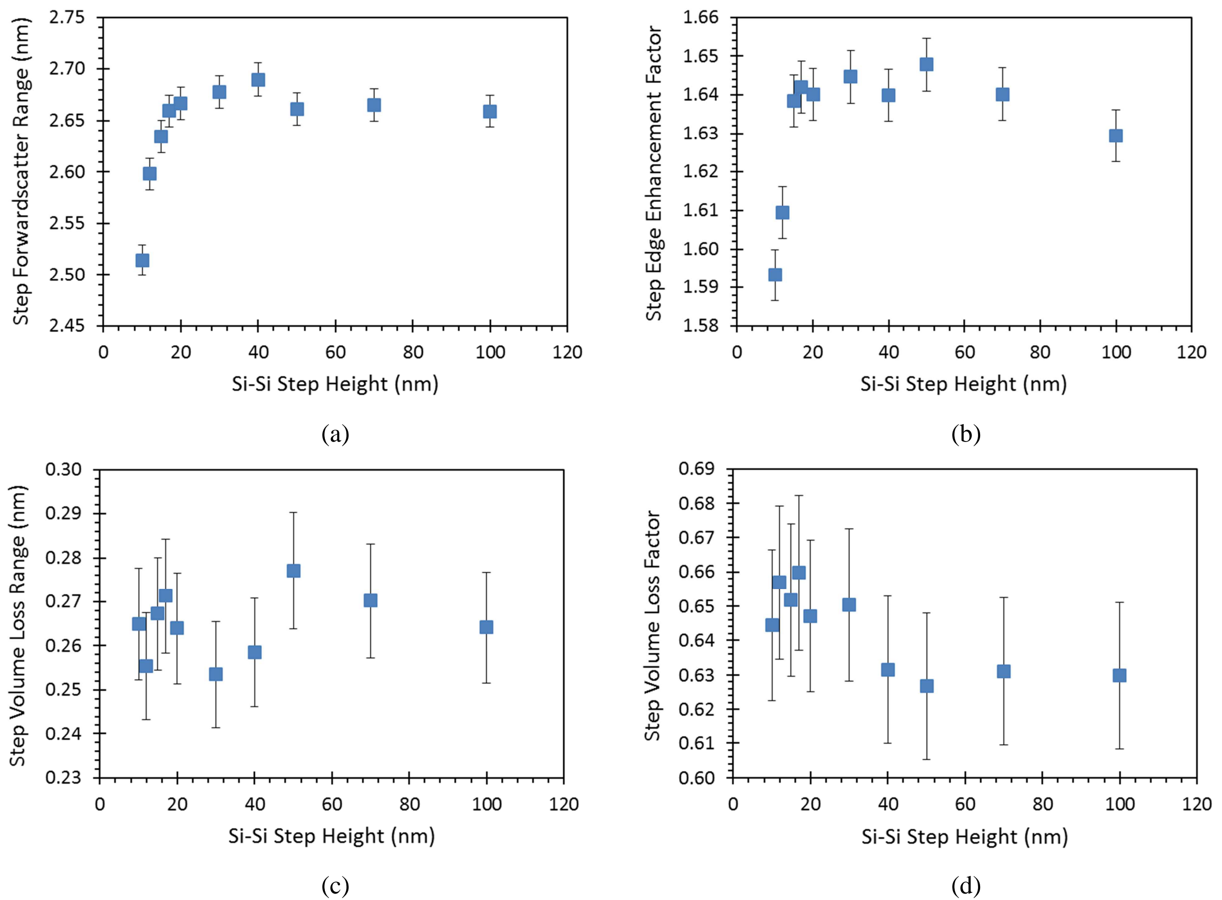

Figure 7. Best fit parameters of equation (9) to rigorous Monte Carlo simulations of an isolated silicon edge at 500 eV landing energy, using a point incident beam, when $x > 0$ (that is, on the top half of the step) for various step heights.

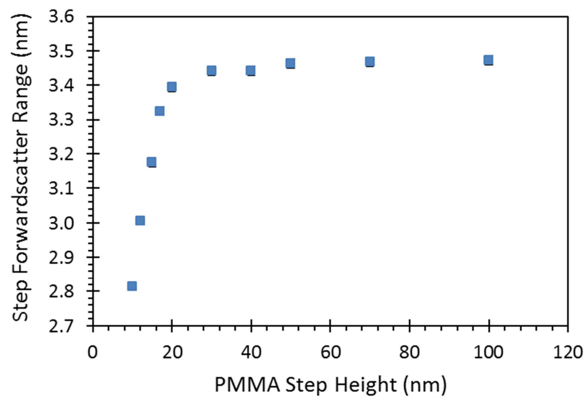

(a)

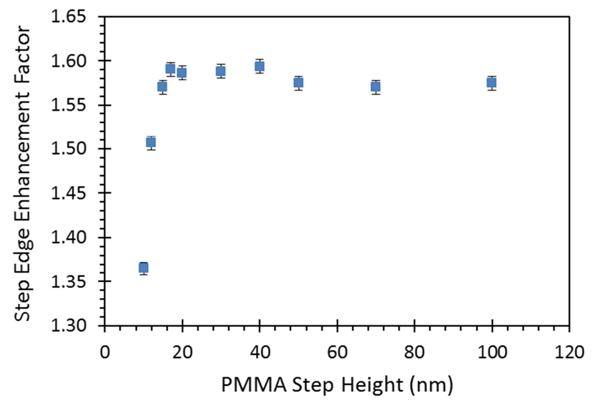

(b)

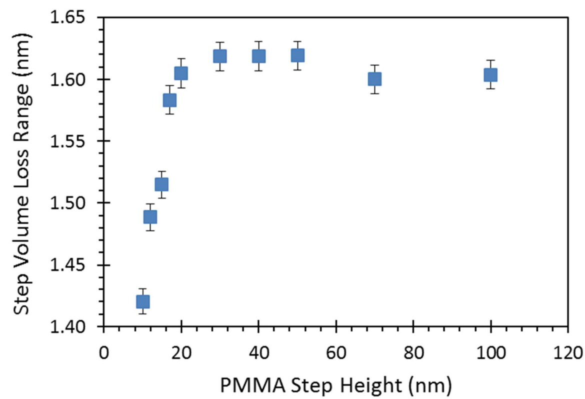

(c)

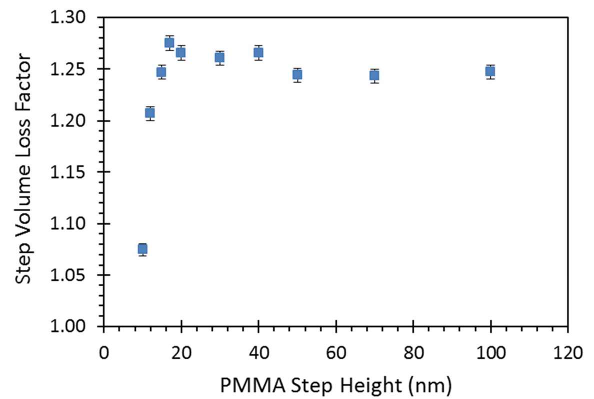

(d)

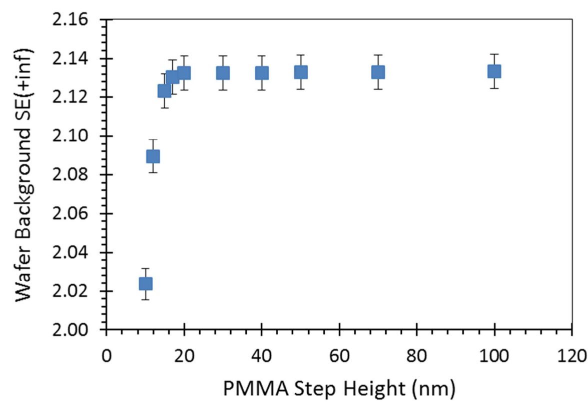

(e)

Figure 8. Best fit parameters of equation (9) to rigorous Monte Carlo simulations of an isolated PMMA edge at 500 eV landing energy, using a point incident beam, when $x > 0$ (that is, on the top half of the step) for various step heights.

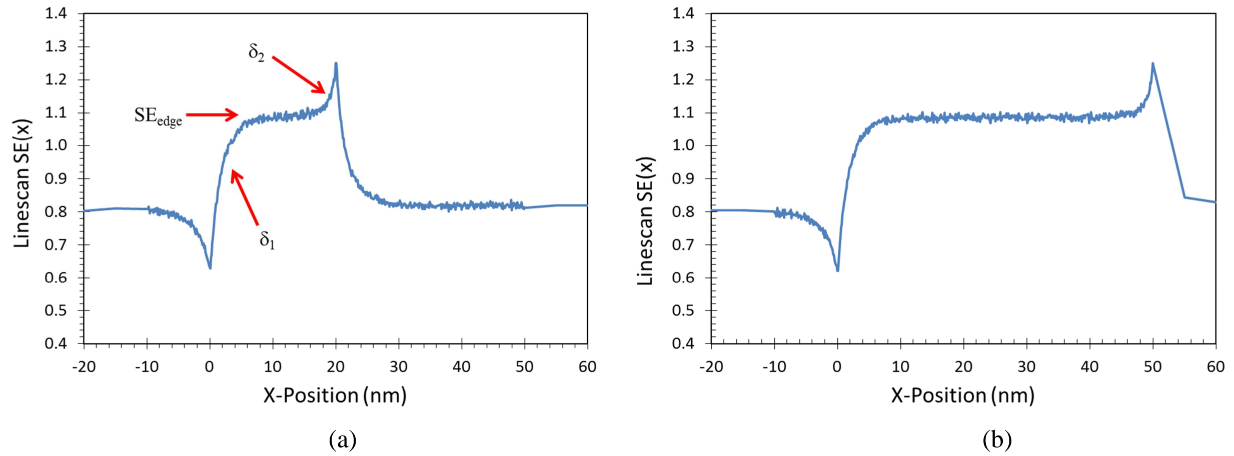

Figure 9. Monte Carlo simulations of an isolated silicon edge with a 45° sidewall angle at 500 V, using a point incident beam, for (a) a 20-nm tall step, and (b) a 50-nm tall step.

Fitting the full linescan model (equations (8), (9), (11) for the wafer, top of step, and sidewall regions, respectively) shows that many of the model parameters are a function of the sidewall angle. In the wafer region, the wafer background signal SE(-∞), wafer forward scatter range σ_f, and wafer backscatter range σ_b are approximately independent of sidewall angle for both step materials. For the silicon step, the wafer backscatter absorption α_b varies approximately as the square of 1-cos(θ) (Figure 10a). As the sidewall angle approaches zero, the step no longer absorbs the secondaries generated by backscattered electrons. For the PMMA step, the negative value of α_b leads to a different, quadratic behavior (Figure 11a). For the silicon step, the wafer forward scatter absorption parameter α_f is approximately independent of sidewall angle, but for the PMMA step it increases approximately linearly with 1-cos(θ) (Figure 11b).

Letting $\tilde{p}$ represent the value of a parameter *p* for a 90° step, the variation of the wafer linescan parameters with sidewall angle take the form

$$\begin{gathered}\sigma_b = s_b h \\ \text{Silicon Step: } \alpha_b = \tilde{\alpha}_b (1-\cos\theta)^2 \\ \text{PMMA Step: } \alpha_b = 0.213(1-\cos\theta)^2 + (\tilde{\alpha}_b - 0.213)(1-\cos\theta) \\ \text{PMMA Step: } \alpha_f = 0.066 + (\tilde{\alpha}_f - 0.066)(1-\cos\theta)\end{gathered} \tag{12}$$

On the top of the step, the step forward scatter range σ_e varies linearly with the square of 1-cos(θ) (Figures 10b and 11c). For the silicon step on a silicon wafer it goes between the wafer forward scatter range when θ = 0° to the step forward scatter range when θ = 90°. The step edge enhancement factor α_e varies linearly with 1-cos(θ) (Figures 10c and 11d). The step volume loss range σ_v is independent of sidewall angle, but the step volume loss factor α_v is highly nonlinear with sidewall angle (Figures 10d and 11e). For the silicon step, the step volume loss factor is zero for angles of 79° and below, then rises roughly as 1-cos(θ) to the fourth power. For the PMMA step, the step volume loss factor goes roughly as 1-cos(θ) to the fourth power over all angles.

$$\text{Silicon Step: } \sigma_e = \sigma_f + (\tilde{\sigma}_e - \sigma_f)(1-\cos\theta)^2$$
$$\text{PMMA Step: } \sigma_e = 3.49 + (\tilde{\sigma}_e - 3.49)(1-\cos\theta)^2$$
$$\alpha_e = \tilde{\alpha}_e(1-\cos\theta) \tag{13}$$
$$\text{Silicon Step: } \alpha_v = -0.48 + (\tilde{\alpha}_v + 0.48)(1-\cos\theta)^4, \ \theta > 79^o$$
$$\text{PMMA Step: } \alpha_v = \tilde{\alpha}_v(1-\cos\theta)^4$$

As for the sidewall region parameters, the value of SE_{edge} is roughly quadratic with 1-cos(θ) with a peak at about 75º – 80º (Figures 10e and 11f). For the silicon step, the decrease in SE_{edge} for the higher angles is small and probably negligible, but for the PMMA edge it is significant. Note that the SE_{edge} behavior observed here is not proportional to 1/cos(θ) as is often assumed. For the silicon step, the length parameters δ_1 and δ_2 are both linear with cos(θ) (Figure 10f). For the PMMA step, δ_1 is linear with cos(θ), but rises much more quickly than for the silicon step (Figure 11g). Unlike the silicon step, δ_2 goes as $\cos^2(\theta)$ for the PMMA step (Figure 11f).

$$\text{PMMA Step: } SE_{edge} = \tilde{S}E_{edge} + 4\cos\theta, \ \theta > 79^o$$
$$\delta_1 = \tilde{\delta}_1 \cos\theta$$
$$\text{Silicon Step: } \delta_2 = \tilde{\delta}_2 \cos\theta \tag{14}$$
$$\text{PMMA Step: } \delta_2 = \tilde{\delta}_2 \cos^2\theta$$

All of these trends can be combined into one equation for the cases where the step height $h \geq 20$ nm and the sidewall angle $\theta \geq 80º$ (for the 500 V case). The resulting best fit parameters over this range of conditions for both a silicon step and a PMMA step are given in Table III. An example of a fit using these parameters is given in Figure 12 for the case of a 20-nm tall PMMA step with an 80º sidewall angle.

Real scanning electron microscopes do not have point beams of electrons impinging on the sample. Instead, the beam is approximately a Gaussian owing to the finite resolution of the microscope and other beam non-idealities. Thus, the expected linescan will be the point linescan model (equations (8), (9), and (11) combined) convolved with a Gaussian. Carrying out this convolution for the case of a 90º step gives[13]

$$\begin{aligned} SE(x) = \frac{SE(-\infty)}{2}\Bigg[& erfc\left(\frac{x}{\sqrt{2}\sigma_p}\right) - \alpha_f e^{\sigma_p^2/2\sigma_f^2} e^{x/\sigma_f} erfc\left(\frac{\sigma_p^2 + x\sigma_f}{\sqrt{2}\sigma_p\sigma_f}\right) - \alpha_b e^{\sigma_p^2/2\sigma_b^2} e^{x/\sigma_b} erfc\left(\frac{\sigma_p^2 + x\sigma_b}{\sqrt{2}\sigma_p\sigma_b}\right)\Bigg] \\ + \frac{SE(\infty)}{2}\Bigg[& erfc\left(\frac{-x}{\sqrt{2}\sigma_p}\right) + \alpha_e e^{\sigma_p^2/2\sigma_e^2} e^{-x/\sigma_e} erfc\left(\frac{\sigma_p^2 - x\sigma_e}{\sqrt{2}\sigma_p\sigma_e}\right) - \alpha_v e^{\sigma_p^2/2\sigma_v^2} e^{-x/\sigma_v} erfc\left(\frac{\sigma_p^2 - x\sigma_v}{\sqrt{2}\sigma_p\sigma_v}\right)\Bigg] \end{aligned} \tag{15}$$

where σ_p is the standard deviation (width parameter) of the incident Gaussian electron beam probe. For the case of a sidewall angle less than or equal to 90º,

$$
\begin{aligned}
SE(x) = {} & \frac{SE(-\infty)}{2}\left[erfc\left(\frac{x}{\sqrt{2}\sigma_p}\right)\right] + \frac{SE(\infty)}{2}\left[erfc\left(\frac{h/\tan\theta - x}{\sqrt{2}\sigma_p}\right)\right] \\
& - \frac{SE(-\infty)}{2}\left[\hat{\alpha}_f e^{x/\sigma_f} erfc\left(\frac{\sigma_p^2 + x\sigma_f}{\sqrt{2}\sigma_p\sigma_f}\right) + \hat{\alpha}_b\, e^{x/\sigma_b} erfc\left(\frac{\sigma_p^2 + x\sigma_b}{\sqrt{2}\sigma_p\sigma_b}\right)\right] \\
& + \frac{SE_{edge}}{2}\left[erfc\left(\frac{-x}{\sqrt{2}\sigma_p}\right) - erfc\left(\frac{h/\tan\theta - x}{\sqrt{2}\sigma_p}\right)\right] \\
& + c_1 e^{-x/\delta_1}\left[erfc\left(\frac{\sigma_p^2 - x\delta_1}{\sqrt{2}\sigma_p\delta_1}\right) - erfc\left(\frac{\sigma_p^2 + (h/\tan\theta - x)\delta_1}{\sqrt{2}\sigma_p\delta_1}\right)\right] \\
& - c_2 e^{-(h/\tan\theta - x)/\delta_2}\left[erfc\left(\frac{\sigma_p^2 + x\delta_2}{\sqrt{2}\sigma_p\delta_2}\right) - erfc\left(\frac{\sigma_p^2 - (h/\tan\theta - x)\delta_2}{\sqrt{2}\sigma_p\delta_2}\right)\right] \\
& + \frac{SE(\infty)}{2}\left[\hat{\alpha}_e e^{(h/\tan\theta - x)/\sigma_e} erfc\left(\frac{\sigma_p^2 + (h/\tan\theta - x)\sigma_e}{\sqrt{2}\sigma_p\sigma_e}\right) - \hat{\alpha}_v\, e^{(h/\tan\theta - x)/\sigma_v} erfc\left(\frac{\sigma_p^2 + (h/\tan\theta - x)\sigma_v}{\sqrt{2}\sigma_p\sigma_v}\right)\right]
\end{aligned}
\tag{16}
$$

where

$$
\begin{aligned}
c_1 &= \frac{1}{2}\left(SE(-\infty)\left[1 - \alpha_f - \alpha_b\right] - SE_{edge}\right) e^{\sigma_p^2/2\delta_1^2} \\
c_2 &= \frac{1}{2}\left(SE(+\infty)\left[1 + \alpha_e - \alpha_v\right] - SE_{edge}\right) e^{\sigma_p^2/2\delta_2^2} \\
\hat{\alpha}_f &= \alpha_f e^{\sigma_p^2/2\sigma_f^2} \\
\hat{\alpha}_b &= \alpha_b\, e^{\sigma_p^2/2\sigma_b^2} \\
\hat{\alpha}_e &= \alpha_e e^{\sigma_p^2/2\sigma_e^2} \\
\hat{\alpha}_v &= \alpha_v\, e^{\sigma_p^2/2\sigma_v^2}
\end{aligned}
$$

The 90⁰ linescan model of equation (15) has 11 physically meaningful parameters (or 10 for the case of a silicon step on a silicon wafer since SE(∞) = SE(-∞)). For the case of a sloped sidewall, three more parameters are added. Not all of the terms in the above equation will prove to be significant, however, depending on the application for the equation. For example, if the Gaussian beam sigma is σ_b = 0.5 nm, a number typical for today's high-end CD-SEMs,[15] then all of the terms of the form $e^{\sigma_p^2/2\sigma^2}$ will be very close to 1 whenever σ > 1 nm, which is the case for every parameter except σ_v for a silicon step. For the PMMA step, the wafer backscatter absorption term is very small, and can easily be neglected with only minor error. Also for the PMMA step, near-normal sidewall angles (greater than 85⁰) result in very small values of δ_2, so that the term multiplied by c_2 can be neglected. Finally, for the case where SE(∞) = SE(-∞), we see that

$$
\frac{SE(-\infty)}{2} erfc\left(\frac{x}{\sqrt{2}\sigma_p}\right) + \frac{SE(\infty)}{2} erfc\left(\frac{-x}{\sqrt{2}\sigma_p}\right) = SE(-\infty) = SE(\infty) \tag{17}
$$

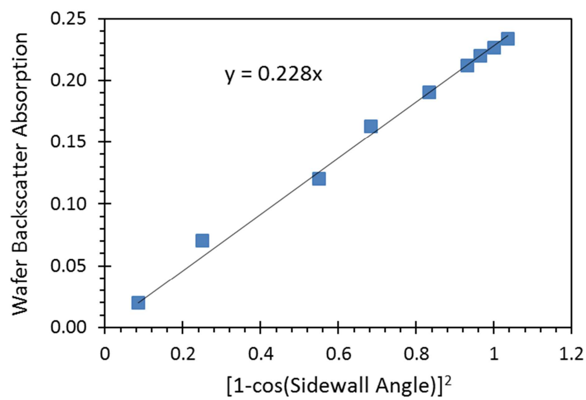

(a)

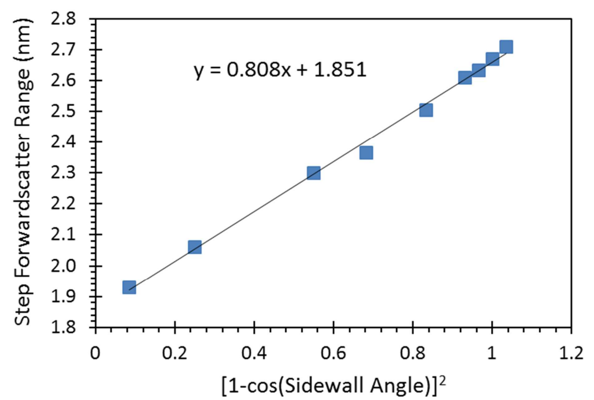

(b)

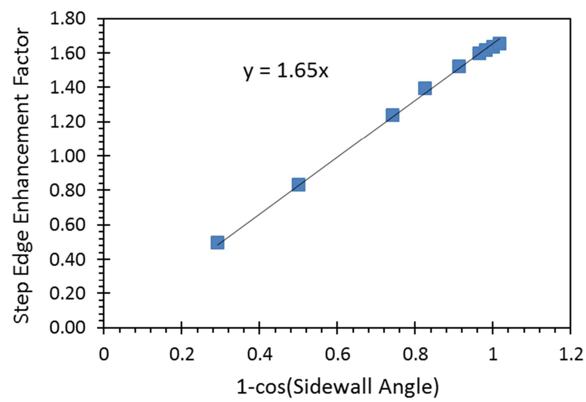

(c)

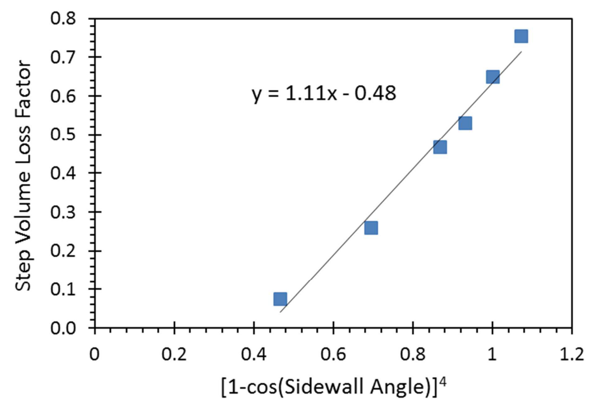

(d)

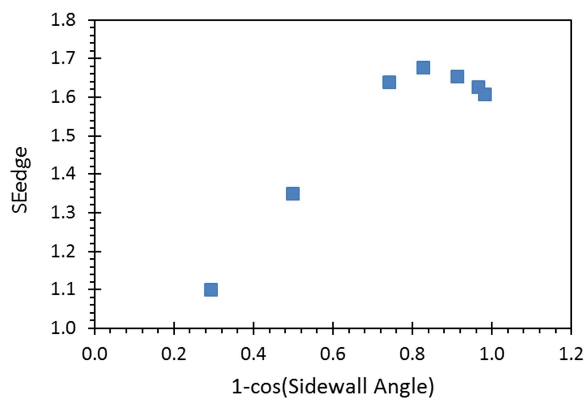

(e)

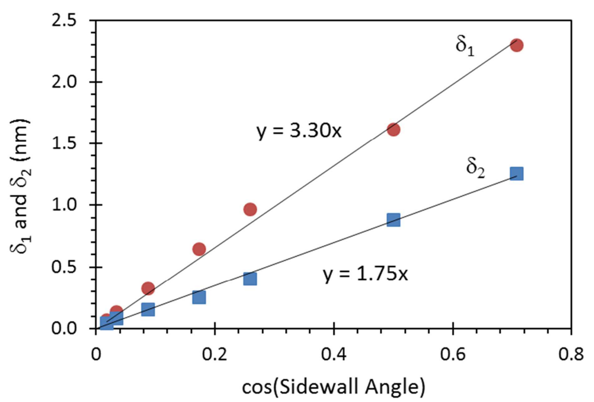

(f)

Figure 10. Best fit parameters of the edge linescan model to rigorous Monte Carlo simulations of an isolated 20-nm tall silicon edge at 500 eV landing energy, using a point incident beam, for various sidewall angles between 45º and 91º.

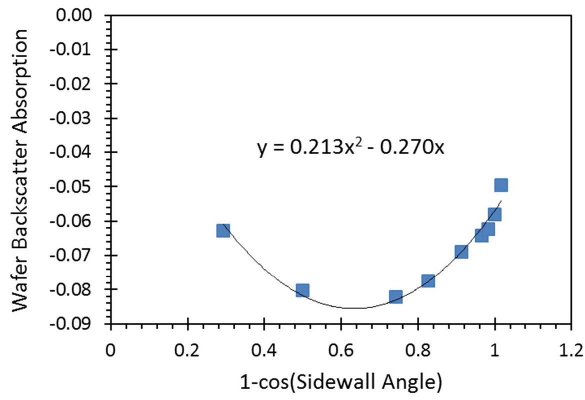

(a)

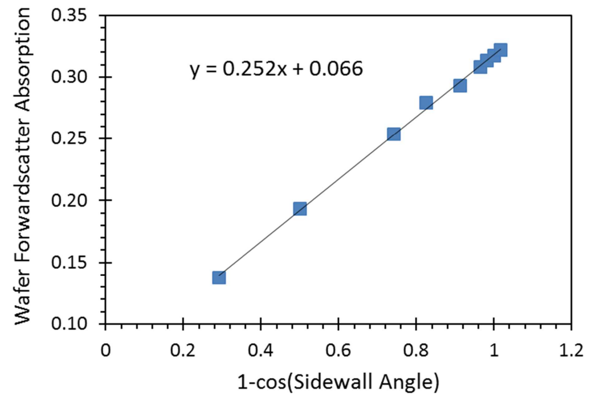

(b)

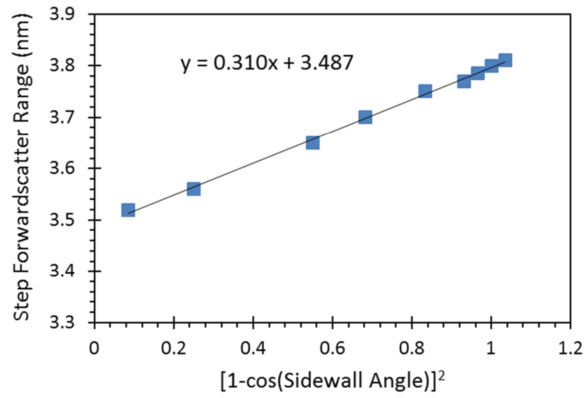

(c)

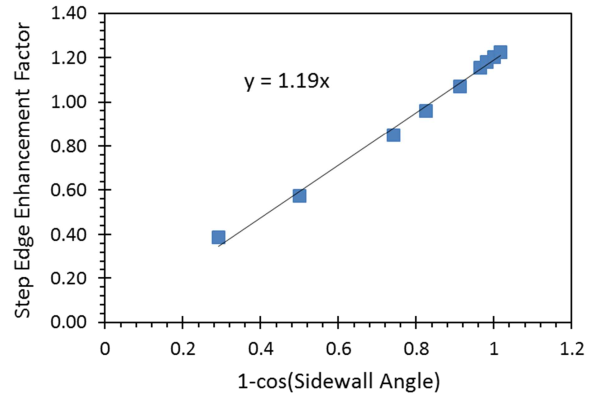

(d)

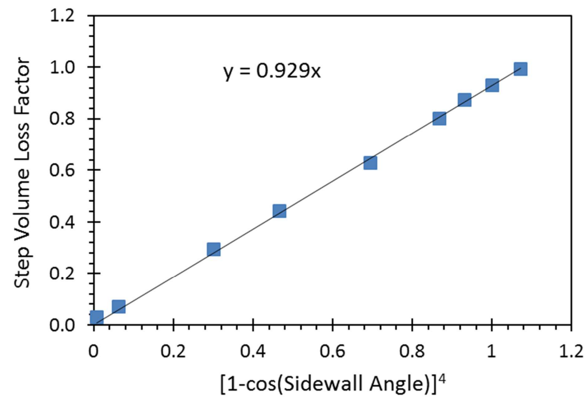

(e)

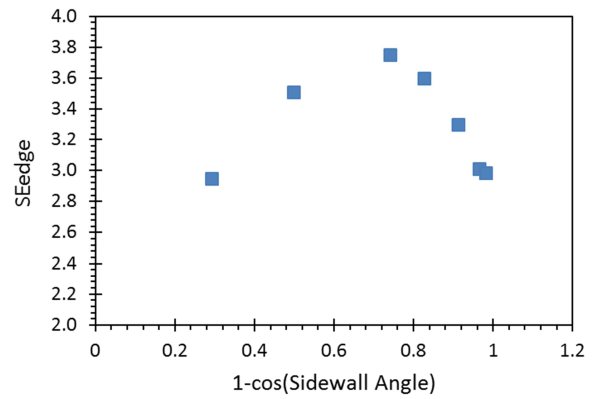

(f)

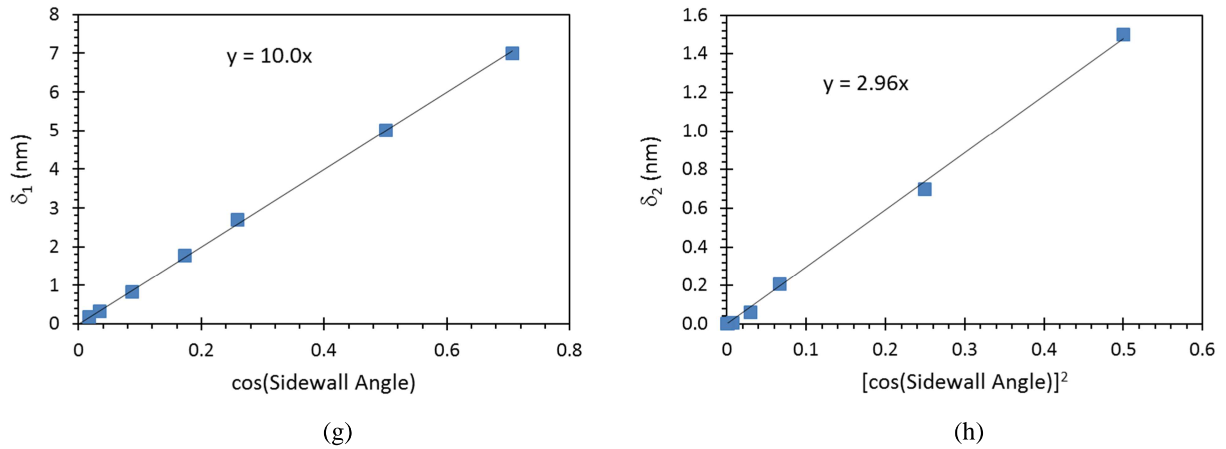

(g) (h)

Figure 11. Best fit parameters of the edge linescan model to rigorous Monte Carlo simulations of an isolated 20-nm tall PMMA edge at 500 eV landing energy, using a point incident beam, for various sidewall angles between 45° and 91°.

Table III. Best fit parameters to rigorous Monte Carlo simulations of an isolated silicon step and PMMA step on a silicon wafer at 500 V electron landing voltage, using a point incident beam.

	Silicon Step	PMMA Step
Si wafer background signal, $SE(-\infty)$	0.817	0.817
Si wafer forward scatter range, σ_f (nm)	1.86	2.24
Si wafer backscatter range per step height, $s_b = \sigma_b/h$	0.90	1.35
Si wafer forward scatter absorption, $\tilde{\alpha}_f$	0.235	0.318
Si wafer backscatter absorption, $\tilde{\alpha}_b$	0.23	–0.057
Step sidewall signal, $\tilde{S}E_{edge}$	1.65	2.9
Step bottom sidewall roll-off distance, $\tilde{\delta}_1$ (nm)	3.3	10
Step top sidewall roll-off distance, $\tilde{\delta}_2$ (nm)	1.75	2.96
Step forward scatter range, $\tilde{\sigma}_e$ (nm)	2.66	3.80
Step volume loss range, σ_v (nm)	0.26	1.24
Step edge enhancement factor, $\tilde{\alpha}_e$	1.65	1.19
Step volume loss factor, $\tilde{\alpha}_v$	0.63	0.93
Step background signal, $SE(\infty)$	0.817	2.13

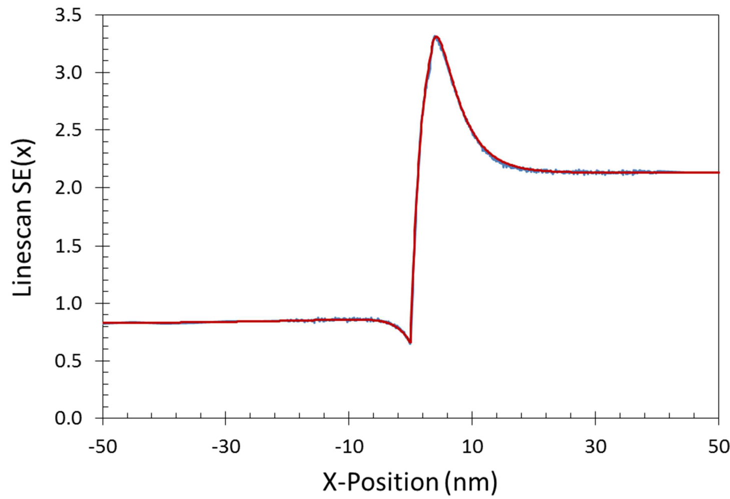

Figure 12. Comparison of the full linescan model of a step (equations (8), (9), and (11) using the angle relationships of equations (12), (13), and (14)) to rigorous Monte Carlo simulations of a 20-nm tall, 80° PMMA edge at 500 V, using a point incident beam. The smooth (red) line is the equation and the jagged (blue) line is the Monte Carlo simulation. RMS error of the fit is 0.013.

4. Derivation of an Approximate Linescan Model for 1-D Features

To first order, one would expect that a feature such as a line or a space could be constructed simply as the combination of two edges, using the ALM for an edge derived in the previous section. We expect this to be true whenever the feature size is large compared to the SEM probe dimension, σ_p. Since this must necessarily be so for any useful metrology, we begin our derivation of the linescan of a feature by properly positioning the linescans of edges. To test this hypothesis, Monte Carlo Simulations of various silicon and PMMA features of various widths, pitches, and thicknesses (heights) were generated. Figure 13 shows an example of a 15-nm wide feature made of 30-nm thick silicon, on a 100-nm pitch (Figure 13a) and a 30-nm pitch (Figure 13b). Added to the graphs are analytical linescan models made by simply combining edges.

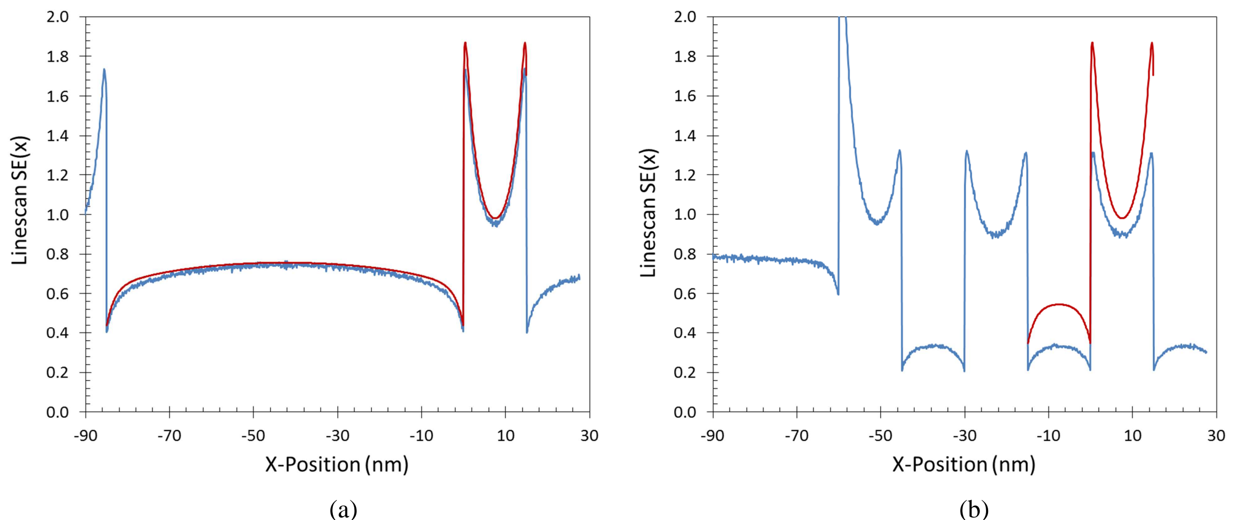

Figure 13. The combination of edge linescans (red smooth curves) are compared to Monte Carlo simulations (blue jagged curves) of 30-nm tall silicon features, each 15-nm wide with 90° sidewalls, at 500 eV landing energy, using a point incident beam, for (a) pitch = 100 nm (RMS error = 0.036), and (b) pitch = 30 nm (RMS error = 0.25).

While the general shape of the ALM matches the Monte Carlo simulation results, there is a lower overall signal for the case of the small 15-nm space compared to the larger 85-nm space. Examining simulations over a range of feature sizes and pitches, it is the size of the space that contributes to this discrepancy for the most part. This can be explained as an added difficulty for electrons to escape from a narrow space (see Figure 1, for example). The linescan model can be made to fit the line/space Monte Carlo data by adjusting two parameters as a function of the space width: the step edge enhancement factor α_e, and the wafer background signal SE(-∞).

Simulations were performed for lines of sizes 7, 10, 15, 20, 30, and 50 nm, and pitches corresponding to dense (spacewidth = linewidth) and a 100-nm pitch, using a 500V point incident beam. For the 50-nm linesize a 120-nm pitch was added. Both silicon and PMMA features were modeled on a silicon wafer, with feature heights of 10, 15, 20, 30, and 50 nm. The sidewall angle was fixed at 90°. Using the edge ALM of the previous section, feature linescans were modeled as the sum of edges, then the parameters step edge enhancement factor α_e and wafer background signal SE(-∞) were adjusted to provide the best fit to the simulation data. Figure 15 shows an example of the results for the case of 30-nm tall, 15-nm wide silicon features. Similarly acceptable fits were obtained for all features except the smallest and densest PMMA features: 7-nm line/space and 10-nm line/space patterns. Examples of these worst-case results are shown in Figure 16. Note that these small features approach and enter the regime where the features become smaller than the electron beam's interaction volume, so that the linescans converge from two peaks to one peak. The ALM proposed here does a very good job of capturing these effects for the 7-nm features.

To build a model from these results, the data from Figure 15 was fit to a stretched exponential:

$$SE_{space}(-\infty) = SE(-\infty)\left(1-e^{-(s/\Delta_1)^{P_1}}\right), \quad \alpha_{e,space} = \alpha_e\left(1-e^{-(s/\Delta_2)^{P_2}}\right) \tag{18}$$

where s is the spacewidth. The best fit values of the length scales Δ_1 and Δ_2, and the powers P_1 and P_2, are found in Table IV.

Table IV. Best fit parameters of equation (18) to rigorous Monte Carlo simulations of different feature sizes and pitches at 500 V electron landing voltage, using a point incident beam.

Feature Height	10 nm	15 nm	20 nm	30 nm	50 nm
Silicon Feature:					
SE(-∞) space length scale Δ_1 (nm)	2.6	6.3	9.2	15.1	26.3
SE(-∞) space power P_1	0.53	0.68	0.96	1.0	1.0
α_e space length scale Δ_2 (nm)	10.0	15.2	19.6	25.9	38.2
α_e space power P_2	0.70	0.67	0.64	0.59	0.49
PMMA Feature:					
SE(-∞) space length scale Δ_1 (nm)	0.11	1.3	3.8	10.4	22.8
SE(-∞) space power P_1	0.25	0.40	0.53	0.68	0.89
α_e space length scale Δ_2 (nm)	2.5	2.2	4.0	3.4	3.1
α_e space power P_2	0.49	0.42	0.50	0.48	0.47

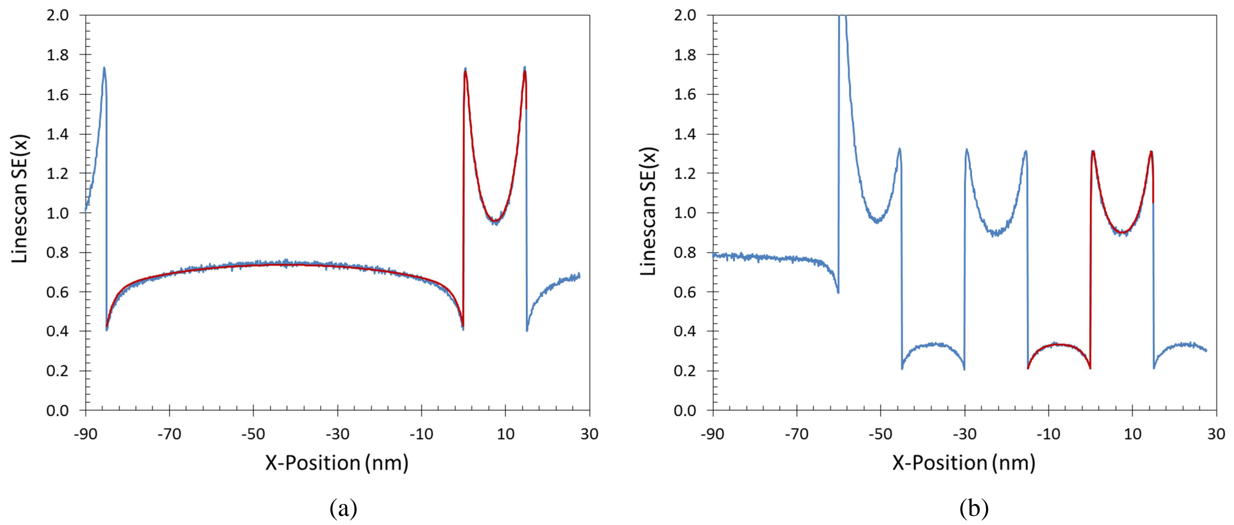

Figure 14. The linescan model made from the combination of two edge linescans (red smooth curves) is adjusted to match the Monte Carlo simulation results (blue jagged curves) by changing the step edge enhancement factor α_e and the wafer background signal SE(-∞). This data, corresponding to the case of Figure 13, is representative of the results obtained (RMS error = 0.012 and 0.014 for (a) and (b), respectively).

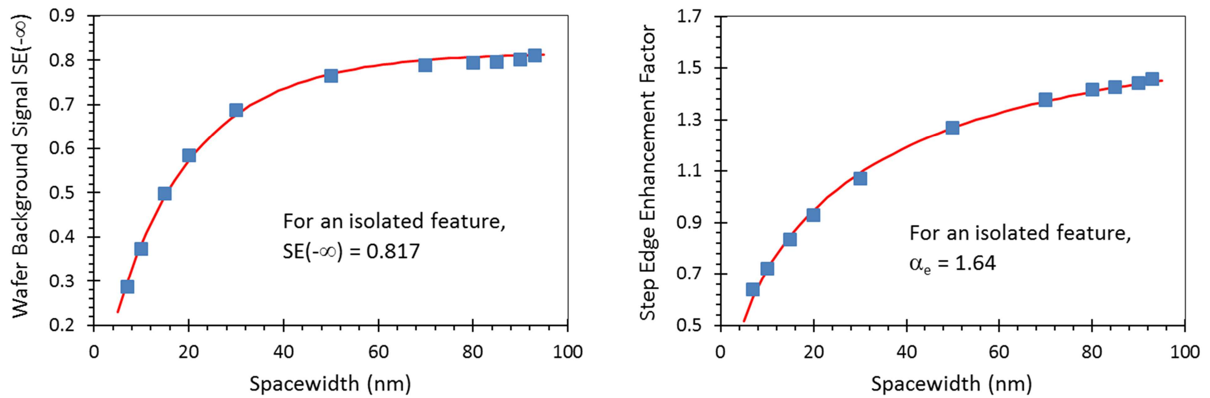

Figure 15. The feature ALM is matched to Monte Carlo results for 30-nm tall silicon features. Shown (symbols) are the best fit values of (a) the step edge enhancement factor α_e, and (b) wafer background signal SE(-∞) as a function of the spacewidth between line features. The curves are fits of equation (18) to these points.

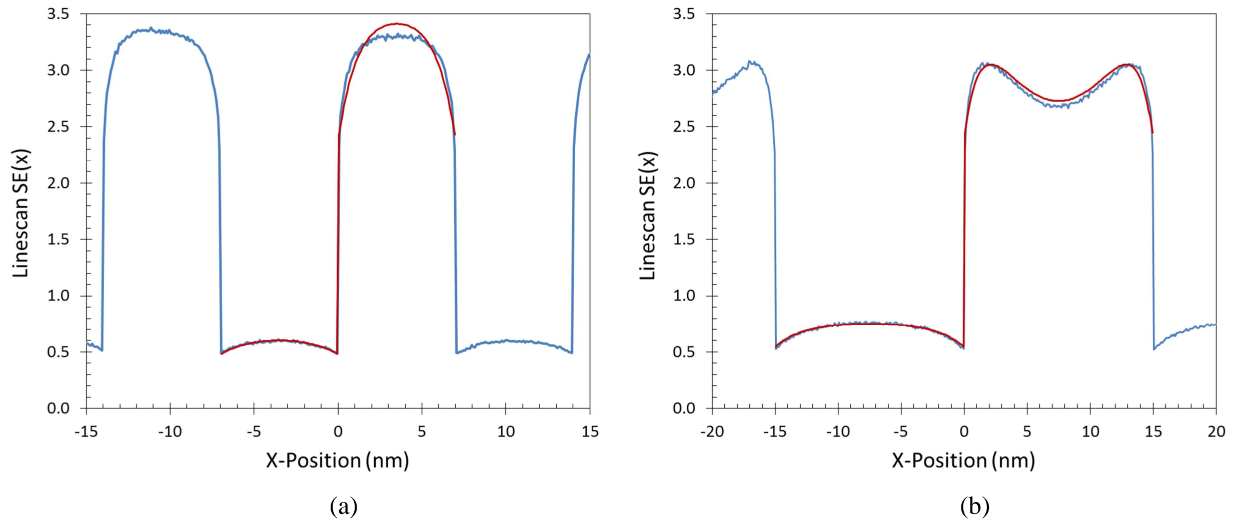

Figure 16. The ALM made from the combination of two edge linescans (red smooth curves) is adjusted to match the Monte Carlo simulation results (blue jagged curves) by changing the step edge enhancement factor α_e and the wafer background signal SE(-∞). Small pitch PMMA lines showed the worst fits, such as (a) 7-nm lines and spaces (RMS error = 0.064), and (b) 15-nm lines and spaces (RMS error = 0.038) for 20-nm tall PMMA features.

5. Stability Test of Approximate Linescan Model for 1-D Features

One important goal of this work is to use the ALM as a more rigorous edge detection and CD measurement algorithm. Given a noisy SEM image, will the linescan model, with material parameters calibrated ahead of time, do a better job of extracting the correct feature size and sidewall angle than conventional edge detection algorithms? To study this, linescans were generated for 500 V beam landing voltage and N = 10000 incident electron per pixel on PMMA line/space features on silicon. The benchmark case will use 10-nm lines on a 20-nm pitch, 30-nm height, and 89º sidewalls. The generated linescans used a 0.01nm beam width (1σ), so the linescans first were convoluted with a 0.5nm 1σ Gaussian beam profile to convert them into realistic linescans representative of contemporary CD-SEM imaging capabilities.[15] Noise with a Gaussian distribution was added to each pixel, in amounts equivalent to the noise expected if the number of incident electrons per pixel were N = 250, 500 or 1000, which roughly covers the dose range commonly used. The noise baseline was computed by repeating one of the cases several times at N = 10000, and adjusted according to the well-known $N^{-1/2}$ dependence. Noise was then doubled yet again, to account for extra error budget due to other potential real-world noise sources that are not comprehended in the JMONSEL modelling (vibrations, electromagnetics, charging, etc.). Examples of these linescans can be seen in Figure 17. Ten linescans were generated for each of the above cases, and for each the ALM was fit adjusting only the CD and sidewall angle, leading to relative values for expected accuracy and precision, as was done in previous works.[12,15]

Various common edge detection algorithms were applied to these virtual SEM linescans. While other algorithms are available, here we apply three of the simpler algorithms: threshold (TH), linear regression to baseline (LR), and maximum derivative (MD). While the TH algorithm is simplistic, it is the most common algorithm in use in the industry, and is very flexible for any waveform since it can be carefully set to target individual details on a waveform. The weakness of TH is its sensitivity to noise variation, but in this simulation study noise is well-controlled. LR is also commonly used, and is interesting as it represents the general class of "curve-fitting" algorithms which are better at handling noise. The MD algorithm is even more vulnerable to noise than TH, but is still used by some users. Details on these algorithms can be seen elsewhere.[4,15] The benchmark linescan with random noise instances was measured by each edge algorithm (10 times each for the analytical linescan model, 1000 times each for the standard algorithms), using no filtering. The output is a sample of CD values (and for the case of the analytical linescan, sidewall angle values as well) with averages and standard deviations, which relate to accuracy and precision. Note that one advantage of working with simulations is that accuracy is knowable since the targets are perfectly defined.

Results are shown in Figure 18 (MD results were excluded from the figure because those results were much worse than the others). The TH algorithm used a 25% threshold, and the LR used a 50% threshold with 20% and 80% lower and upper fulcrums. Relative precision is equivalent to the edge detection reproducibility σ_ε discussed elsewhere.[4,15]**Error! Bookmark not defined.**

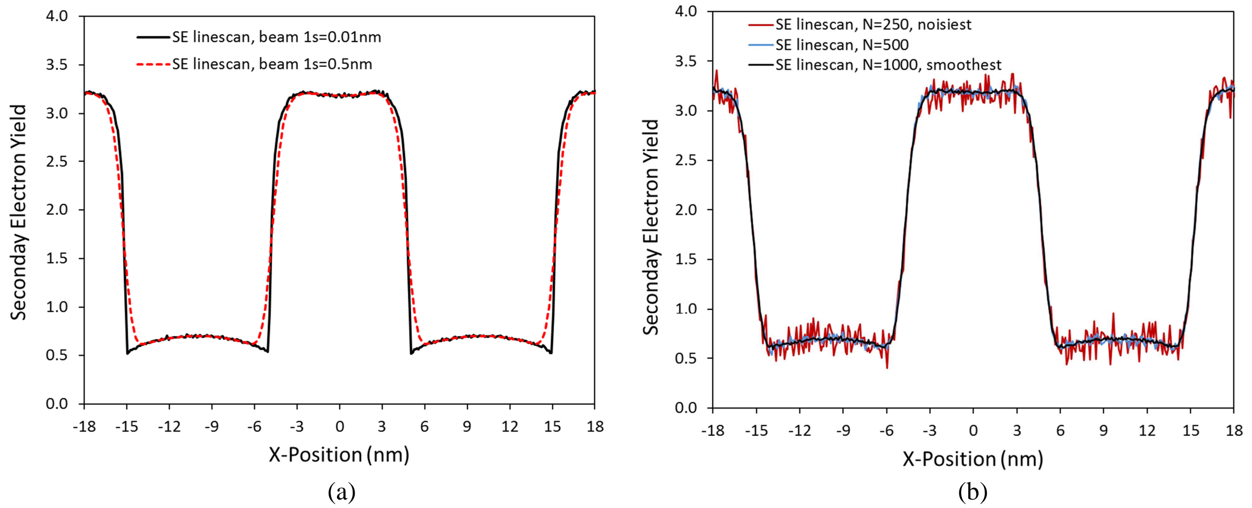

Figure 17. Simulated linescans at 500 V for 10-nm wide PMMA lines of 20-nm pitch and 30-nm height with 89º sidewall angle: (a) the base linescans using N=10000 electrons per pixel, with a perfect beam (solid black line) and the convoluted 0.5-nm beam (red dashed line), and (b) convoluted beam with added noise instances.

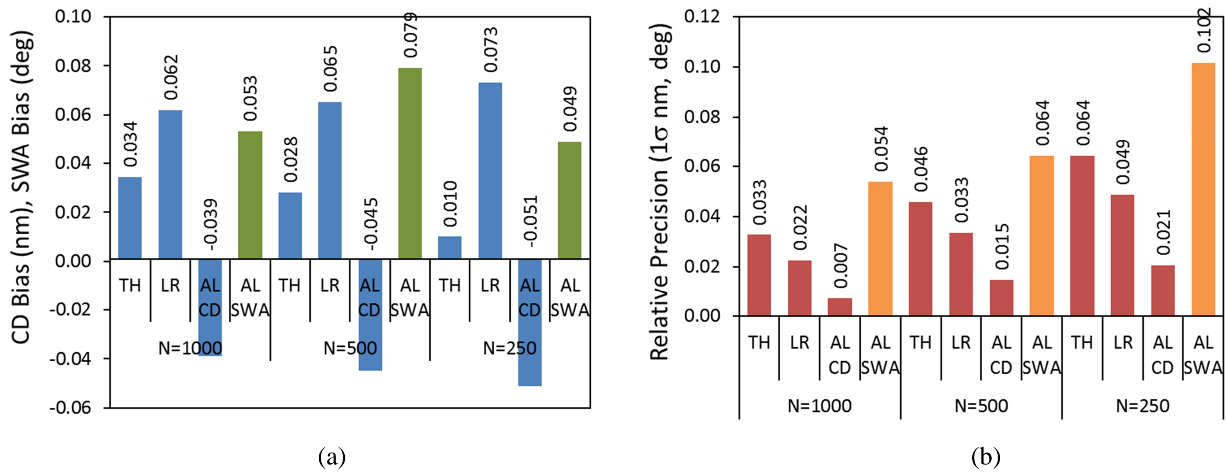

Figure 18. Comparison of performance of different algorithms for CD measurement of features in Figure 17 (TH = threshold, LR = linear regression, AL = analytical linescan model): (a) CD bias, and (b) relative CD precision, σ_ε.

6. Conclusions and Future Work

The analytical linescan model (ALM) that has been developed in this work offers several important advantages. After calibration against a rigorous Monte Carlo simulator for the various materials involved in the sample, the ALM can, with quite reasonable accuracy, predict the linescans of those materials for a wide variety of geometric shapes. In particular, for feature thicknesses of greater than 20 nm (for the case of a 500 eV landing energy) and sidewall angles greater than 80°, the calibrated ALM matches the Monte Carlo simulated secondary electron waveforms over a wide range of feature sizes, pitches, thickness, and sidewall angles. While only silicon and PMMA features on silicon wafers were tested, it is expected that similar calibration procedures would yield similar results for a wide variety of materials. Since the model is based on reasonable physical assumptions and uses physically-based parameters, both interpolations and extrapolations to a wide range of geometries should prove possible.

One possible use of the ALM is as a physics-based edge detection/linewidth measurement algorithm. While the results presented here are preliminary, they are sufficiently encouraging to hope that such an application could become practical with further effort. It is likely that the complete ALM presented here could be greatly simplified when working in the real world of noisy images and moderately wide beams. Other real-world effects, such as baseline drift and intensity scale variation, must also be added to the model to make it practical in the field. Additionally, a robust calibration procedure must be developed if routine use of the ALM is envisioned. Finally, extensive testing using experimental SEM images would be required. While the work remaining is extensive, the promise of a physically based linescan measurement algorithm with improved accuracy and precision for both CD and sidewall angle for feature sizes of 10 nm and below might justify the effort.

7. Acknowledgements

First and definitely most, we would like to thank John Villarrubia of NIST for his writing and continued support of the JMONSEL SEM simulator code, and also for many insightful discussions on its use, on edge detection and model-based algorithms, and CD metrology and simulation studies in general. Discussions with Dr. Brad Thiel, CNSE Professor assignee to SEMATECH have also been helpful in the area of SEM simulation and SEM spot size, and Matt Malloy, Brian Sapp and Kevin Cummings for general support. Abner Bello and Alok Vaid or GLOBAL FOUNDRIES, Eric Solecky, Narender Rana and Erin McLellan-Lavigne of IBM, Chris Deeb of Intel, and Toru Ikegami and Alex Danilevsky of Hitachi-High Tech are thanked for discussions which directly inspired this effort, whether they knew it or not. Additionally, we would like to thank Amie Kaplan, Peter DiFondi, Cody Teague, Mark Porter and Stacy Stringer of SEMATECH for help in finding and establishing much-needed computational resources for the JMONSEL simulations, and also to Chandra Sarma of SEMATECH (Intel assignee) for loaning further computational resources. We also would like to give much thanks to the SEMATECH Combined Metrology Advisory Group (XMAG) and the SEMATECH Metrology Program Advisory Group (MPAG) for their continuing support of this project.

8. References

[1] J. S. Villarrubia, N. W. M. Ritchie, and J. R. Lowney, “Monte Carlo modeling of secondary electron imaging in three dimensions”, *Proc. SPIE*, **6518**, 65180K (2007).
[2] J. S. Villarrubia, and Z. J. Ding, “Sensitivity of SEM width measurements to model assumptions”, *J. Micro/Nanolith. MEMS MOEMS*, **8**, 033003 (2009).
[3] J. S. Villarrubia, A. E. Vladár, B. Ming, et al., “Scanning electron microscope measurement of width and shape of 10 nm patterned lines using a JMONSEL-modeled library”, *Ultramicroscopy*, **154**, 15 (2015).
[4] J. S. Villarrubia, A. E. Vladár, and M. T. Postek, “Simulation study of repeatability and bias in the critical dimension scanning electron microscope”, *J. Microlith. Microfab. Microsyst.,* **4**(3), 033002 (Jul–Sep, 2005).
[5] B. Bunday, T. Germer, V. Vartanian, A Cordes, A. Cepler, and C. Settens, “Gaps Analysis for CD Metrology Beyond the 22 nm Node”, *Proc. SPIE*, **8681**, 86813B (2013).

[6] Narender Rana, Yunlin Zhang, Taher Kagalwala, and Todd Bailey, "Leveraging advanced data analytics, machine learning, and metrology models to enable critical dimension metrology solutions for advanced integrated circuit nodes", *J. Micro/Nanolith. MEMS MOEMS*, **13**(4), 041415 (2014).
[7] M. P. Davidson and A. E. Vladár, "An inverse scattering approach to SEM line width measurement", *Proc. SPIE*, **3677**, 640–649 (1999).
[8] J. S. Villarrubia, A. E. Vladár, J. R. Lowney, and M. T. Postek "Edge determination for poly-crystalline silicon lines on gate oxide", *Proc. SPIE*, **4344**, 147–156 (2001).
[9] J. S. Villarrubia, A. E. Vladár, J. R. Lowney, and M. T. Postek, "Scanning electron microscope analog of scatterometry", *Proc. SPIE*, **4689**, 304–312 (2002).
[10] J. S. Villarrubia, A. E. Vladár, B. D. Bunday, and M. Bishop, "Dimensional metrology of resist lines using a SEM model-based library approach", *Proc. SPIE*, **5375**, 199–209 (2004).
[11] J. S. Villarrubia, A. E. Vladár, and M. T. Postek, "Simulation study of repeatability and bias in the critical dimension scanning electron microscope", *J. Microlith. Microfab. Microsyst.*, **4**(3), 033002 (Jul–Sep 2005).
[12] Chie Shishido, Maki Tanaka, and Mayuka Osaki, "Accurate measurement of very small line patterns in critical dimension scanning electron microscopy using model-based library matching technique", *J. Micro/Nanolith. MEMS MOEMS*, **10**(1), 013010 (2011).
[13] Benjamin D. Bunday and Chris A. Mack, "Influence of Metrology Error in Measurement of Line Edge Roughness Power Spectral Density", *Metrology, Inspection, and Process Control for Microlithography XXVIII, Proc*., SPIE Vol. **9050**, 90500G (2014).
[14] Carl Georg Frase, Egbert Buhr, and Kai Dirscherl, "CD characterization of nanostructures in SEM metrology", *Meas. Sci. Technol*. **18**(2), 510–519 (2007).
[15] Benjamin Bunday, Aron Cepler, Aaron Cordes, and Abraham Arceo, "CD-SEM metrology for sub-10 nm width features", *Metrology, Inspection, and Process Control for Microlithography XXVIII, Proc*., SPIE Vol. **9050**, 90500T (2014).